ENVIRONMENTAL RESEARCH
LETTERS

LETTER • OPEN ACCESS

Effects of the South Asian summer monsoon anomaly on interannual variations in precipitation over the South-Central Tibetan Plateau

To cite this article: Yanxin Zhu *et al* 2020 *Environ. Res. Lett.* **15** 124067

Environmental Research Letters

CrossMark

OPEN ACCESS

RECEIVED
9 December 2019

REVISED
29 October 2020

ACCEPTED FOR PUBLICATION
3 November 2020

PUBLISHED
16 December 2020

LETTER

Effects of the South Asian summer monsoon anomaly on interannual variations in precipitation over the South-Central Tibetan Plateau

Yanxin Zhu[1,2], **Yan-Fang Sang**[1,5], **Deliang Chen**[3], **Bellie Sivakumar**[4] and **Donghuan Li**[1]

[1] Key Laboratory of Water Cycle & Related Land Surface Processes, Institute of Geographic Sciences and Natural Resources Research, Chinese Academy of Sciences, Beijing, People's Republic of China
[2] University of Chinese Academy of Sciences, Beijing, People's Republic of China
[3] Regional Climate Group, Department of Earth Sciences, University of Gothenburg, Gothenburg, Sweden
[4] Department of Civil Engineering, Indian Institute of Technology Bombay, Powai, Mumbai 400076, India
[5] Author to whom any correspondence should be addressed.

E-mail: sangyf@igsnrr.ac.cn **and** sunsangyf@gmail.com

Keywords: Tibetan Plateau, precipitation anomaly, South Asian summer monsoon, water vapor transport, moisture budget analysis

Supplementary material for this article is available online

Abstract

An anomalous South Asian summer monsoon (SASM) system could generate a large anomaly in precipitation and hydrological disasters in the SASM-prevailing area, as widely reported for the Indian Peninsula. However, how the SASM system influences the precipitation anomaly over the South-Central Tibetan Plateau (SCTP) is largely unknown. In this study, we (a) analyze the influences of the early and late onset (demise) of the SASM on the interannual variations in precipitation over the SCTP during 1979–2015; and (b) illuminate the underlying mechanisms and asymmetric effects with regard to the onset and demise of the SASM by analyzing the characteristics of water vapor transport and moisture budgets in this region. Results indicate that the precipitation anomaly over the SCTP is dominated by the cyclonic and anticyclonic water vapor transport associated with the anomalous SASM activities, causing moisture convergence and divergence in this region. The topographic effect in the southeastern Tibetan Plateau (SETP) and southwestern Tibetan Plateau (SWTP) further strengthens the anomaly in water vapor transport in vertical direction and contributes to the precipitation anomaly through moisture convergence and divergence. The anomalous SASM and topography exhibit asymmetric effects between the onset and demise as well as between the early and late onset (demise) of the SASM. They cause 23.41%, 15.91%, and 1.96% difference in precipitation between the early and late SASM-onset years, and 13.05%, 21.50%, and 29.86% difference in precipitation between the early and late SASM-demise years in the SETP, central Tibetan Plateau (CETP), and SWTP, by regulating the horizontal and vertical thermodynamic and dynamic processes. The results help improve our understanding of the SASM-precipitation relationship over the SCTP and guide the prediction of precipitation and alleviation of water-related disasters in the region and its surroundings that are home to billions of people in Asia.

1. Introduction

The South Asian summer monsoon (SASM) system is one of the most energetic regional monsoon systems. The onset and demise timings of the SASM system, controlled by the land–ocean meridional thermal contrasts (Li and Yanai 1996, Wang *et al* 2001), determine the propagation, duration, and total amount of precipitation through thermodynamic and dynamic processes in the SASM-prevailing areas (Xavier *et al* 2007, Sabeerali and Ajayamohan 2018). Particularly, anomalous onsets and demises of the SASM are connected to many factors, including the El Niño and La Niña events (Xiang and Wang 2013, Roxy *et al* 2015), local sea surface temperature (SST) (Sabeerali *et al* 2012, Xing *et al* 2016a), snow accumulation anomalies over the Tibetan Plateau (TP) (Fasullo and Webster 2003), and others. They could change the thermodynamic and dynamic processes and generate a large anomaly in precipitation over the SASM-prevailing areas (Goswami and Xavier 2005, Xing *et al* 2016b). For example, the India Meteorological Department reported that the earlier than normal onset of the SASM in 2013 caused precipitation surplus by 6% in the Indian Peninsula, accompanied by serious flooding disasters, while its late onset in 2014 led to precipitation deficit by 12% and drastic droughts (Pai and Bhan 2014, 2015).

The South-Central TP (SCTP), known as the 'Asian water tower', is the origin of several major Asian rivers, including the Yellow River, Yangtze River, Brahmaputra River, Mekong River, and the Indus River, providing a huge amount of freshwater for ecosystems and billions of people in Asia (Immerzeel *et al* 2010). It is widely known that the SCTP is controlled by the SASM system in summer (Chen *et al* 2012, Feng and Zhou 2012, *Yao et al*, 2013), accounting for approximately 60% of annual precipitation (Tong *et al* 2014, Ma *et al* 2018), but with significant spatiotemporal heterogeneity due to the complex topographic and geographic conditions (Yang *et al* 2011, 2014, Curio and Scherer 2016, *Sang et al* 2016). Recent studies have found that precipitation in May has been increasing over the southeastern and central area of the TP, accelerating the lake expansion, wetting, and greening of the TP in recent decades (Chen and You 2017, Zhang *et al* 2017, Liu *et al* 2019). Further, the increasing trends in precipitation in May in these two regions are mainly attributed to the advanced SASM onset, which is connected to the thermodynamic and dynamic adjustment caused by the SST anomaly of the Indian Ocean (Xing *et al* 2016a). Thus far, most studies have focused on the effects and physical causes of the linear trend of SASM onset over the SCTP, while little attention has been paid to the question as to how both anomalous onset and anomalous demise of the SASM influence the interannual precipitation variation in this region. In particular, the spatial manifestation of thermodynamic and dynamic mechanisms for the interannual precipitation variation is largely unknown. Adequate knowledge about these mechanisms is critical for sustainable freshwater management in this region and surrounding areas.

In the present study, we aim to illuminate the influences of the early and late onset (demise) of the SASM system on the interannual variations in precipitation and their underlying mechanisms over the SCTP. The precipitation data from the APHRODITE (Asian Rainfall Highly-Resolved Observational Data Integration Towards Evaluation of Water Resources) and the ERA5 reanalysis data, during 1979–2015 in the SASM-prevailing areas are used in this study. The composite analysis is used to investigate the influences of the early and late onset (demise) of the SASM on precipitation variations, and the moisture budget analysis is used to reveal the physical mechanisms governing the precipitation anomaly. The present study is designed to address the following specific questions by considering the SASM-precipitation dynamics: (a) How do the onset and demise of the SASM control the interannual variations in precipitation over the SCTP? (b) Is there an asymmetric effect of the SASM on SCTP precipitation between its onset and demise, and between its early and late onset (demise)? and (c) What are the underlying mechanisms that are responsible for the variations in interannual precipitation?

2. Data and methods

2.1. Study area

The TP is under the joint influences of the westerlies, SASM, and the East Asian summer monsoon (EASM) system (Webster *et al* 1998, Schiemann *et al* 2009). In summer, the TP is considered as being controlled by the monsoons to the south of 30°N, which then gradually weakens from the 30°N to 35°N before transforming into the prevailing westerlies to the north of 35°N (Yao *et al* 2013). The eastern part of the TP is particularly influenced by the EASM (Cherchi *et al* 2011). The present study focuses on the SASM-dominated SCTP (in the south of 35°N and west of 100°E, as shown in figure S1 (available online at https://stacks.iop.org/ERL/15/124067/mmedia)) as the study area.

2.2. Data

Due to the complex topography, weather, and environment, the existing meteorological stations over the TP are sparse and unevenly distributed (Wang and Zeng 2012). The scarcity in observed data causes great difficulties for hydroclimatic studies in this region. To overcome such difficulties, many studies use remote sensing data and reanalysis data as alternatives (Feng and Zhou 2012, Tong *et al* 2014). However, there are many uncertainties in these two types of data that should be carefully evaluated for reliable outcomes (Wang and Zeng 2012).

For the present study, we collect 13 precipitation datasets from different sources (see Table S1) and compare them with the gauged precipitation data at 80 stations for evaluating their quality. For evaluation, we consider the monthly, seasonal, and interannual variations in precipitation, as well as their spatial heterogeneity. Results indicate that, among the 13 datasets, the APHRODITE matches best with the gauged precipitation observations. The APHRODITE is regarded as the only long-term, continental-scale daily precipitation product that contains a dense network of daily rain gauge data for Asia, at a $0.25° \times 0.25°$ grid spacing, including the SCTP and the SASM-prevailing South Asia (Yatagai *et al* 2012). Many studies have verified its quality (Feng and Zhou 2012, Tong *et al* 2014, Zhu and Sang 2018). By considering its length and completeness, we choose the APHRODITE data from 1979 to 2015 for this study. We further use the ERA5 reanalysis data (with a 0.25° × 0.25° spatial resolution) over the same period, to explore the thermodynamic and dynamic processes of precipitation anomaly caused by changes in the onset and demise of the SASM.

2.3. Methods

2.3.1. Definition of onset and demise times of the SASM system

To quantitatively describe the evolution of the SASM system, various methods have been proposed to define the onset and demise of the SASM system based on precipitation or atmospheric thermodynamic and dynamic conditions in the SASM-prevailing area (Wang and Linho 2002, Fasullo and Webster 2003, Xavier *et al* 2007, Walker and Bordoni 2016). Definition of the onset and demise times of the SASM is critical for the present study. Here, we define them using the objective method proposed by Noska and Misra (2016). The method has the advantage of simplicity, as it uses only one variable, namely the spatially averaged precipitation in a typical region. This way, it avoids the use of upper air variables from the reanalysis or satellite retrievals that may be biased (Noska and Misra 2016). Moreover, it offers the flexibility to adapt to any desired spatial scale based on the needs of the users and allows us to understand the detailed variations of the SASM system (Misra *et al* 2018).

Considering the pathway of the climatological evolution of the SASM system (Wang and Linho 2002), the SASM generally breaks out in the Bay of Bengal (BOB), then moves northwestward, and finally retreats reversely from the northwestern Indian Peninsula (NWIP) (figure S1). Thus, we use the ERA5 precipitation data in the BOB (10°–18°N, 84°–94°E) to define the onset of the SASM, and use the APHRODITE precipitation data in the NWIP (25°–30°N, 75°–80°E) to define its demise. Note that the APHRODITE data does not cover the BOB.

The calculations for the onset and demise times of the SASM are described as follows:

(a) Use the ERA5 data to calculate the daily areal average precipitation in the BOB for day n of year m, denoted as $D_m(n)$;

(b) Calculate the daily cumulative anomaly $D'_m(n)$ of $D_m(n)$

$$D'_m(n) = \sum_{n=1}^{N} \left[D_m(n) - \overline{\overline{D}} \right] \tag{1}$$

with

$$\overline{\overline{D}} = \frac{1}{MN} \sum_{m=1}^{M} \sum_{n=1}^{N} D_m(n) \tag{2}$$

where $\overline{\overline{D}}$ is the average daily precipitation over N (=365/366) days for M (=37) years;

(c) Define the onset date (denoted as SASM-OD) of the SASM as the day when $D'_m(n)$ reaches its absolute minimum value, after the first four months and before the last three months of a year; and

(d) Use the APHRODITE dataset to calculate $D_m(n)$ and $D'_m(n)$ in the NWIP using equations (1) and (2). Then, define the demise date (SASM-DD) of the SASM as the day when $D'_m(n)$ reaches its absolute maximum after the SASM-OD.

The onset and demise dates of the SASM determined by the above method are shown in figure S2. Note that the onset results from the ERA5 reanalysis data keep consistence with those in its adjacent land and also previous studies (Zhang *et al* 2017) (figure S3). Furthermore, we choose the years with the SASM-OD/SASM-DD being lower (higher) than one-standard deviation of its average values (1979–2015) as the typical early (late) SASM-onset/demise years (figure S2). Based on this, the early SASM-onset years are 1995, 2001, 2004, 2007, and 2008, and the late SASM-onset years are 1979, 1986, 1987, 1992, and 1996. The early SASM-demise years are 1979, 1981, 1986, 2001, and 2015, while the late SASM-demise years are 1983, 1985, 1998, 1999, 2004, 2009, and 2013.

We also use the above method to determine the onset and demise of grid precipitation over the SCTP. Moreover, we take the days from the OD to DD as the season length (SL) of grid precipitation to reflect its duration, and use the total amount of the seasonal precipitation (SP) between the OD and DD to reflect the strength of grid precipitation. We use these four indexes to quantify the interannual variations in precipitation over the SCTP and analyze their correlations with the onset/demise of the SASM. We further analyze the changes in the SL and SP (to quantify their anomalies) of precipitation over the SCTP in the early (late) SASM-onset/demise years, for investigating the influence of the SASM anomaly.

2.3.2. Moisture budget analysis

We apply the moisture budget analysis to explore the physical mechanisms governing the precipitation anomaly caused by the early and late onset (demise) of the SASM. Since precipitation (P) is balanced with convergence of vertically integrated atmospheric moisture flux and evaporation on the monthly and longer timescales, the moisture budget equation can be described as follows (Trenberth and Guillemot 1995, Seager *et al* 2010, Seager and Henderson 2013):

$$P = -\frac{1}{g\rho} \int_0^{p_s} \nabla \cdot (Vq)\, dp - \frac{1}{g\rho} \int_0^{p_s} \frac{\partial(\omega q)}{\partial p} dp + E \tag{3}$$

where g is gravitational acceleration, ρ is the density of water, p is the air pressure, p_s is the surface air pressure, V is the horizontal wind vector, ω is the vertical velocity, and q is the specific humidity. The first term (on the right hand side of equation (3)) is referred to as the horizontal moisture convergence, the second term as the vertical moisture convergence, and the final term as the surface evaporation (E).

We then divide P, E, V, ω, and q into monthly means ($\overline{P}$, $\overline{E}$, $\overline{V}$, $\overline{\omega}$, and $\overline{q}$) and departures from the monthly mean (P', E', V', ω', and q') as

$$P = \overline{P} + P',\ E = \overline{E} + E',\ V = \overline{V} + V',\\ \omega = \overline{\omega} + \omega' \text{ and } q = \overline{q} + q'. \tag{4}$$

In many previous studies, the changes in the quadratic nonlinear term have generally been ignored, due to their small amplitude (Seager *et al* 2010, Seager and Henderson 2013). Following this practice, the precipitation anomaly (P') can be expressed as follows:

$$P' = -\frac{1}{g\rho}\int_0^{p_s} \nabla\cdot\left(\overline{V}q'\right)dp - \frac{1}{g\rho}\int_0^{p_s}\nabla\cdot\left(V'\overline{q}\right)dp\\ -\frac{1}{g\rho}\int_0^{p_s}\frac{\partial\left(\overline{\omega}q'\right)}{\partial p}dp - \frac{1}{g\rho}\int_0^{p_s}\frac{\partial\left(\omega'\overline{q}\right)}{\partial p}dp + E' \tag{5}$$

where the first term is referred to as the horizontal thermodynamic component (i.e. the changes in horizontal specific humidity), the second term as the horizontal dynamic component (i.e. the changes in horizontal wind flow), the third term as the vertical thermodynamic component (i.e. the changes in vertical specific humidity), the fourth term as the vertical dynamic component (i.e. the changes in vertical velocity), and the final term as the surface evaporation component. Analysis of the changes in these five components in the early (late) SASM-onset/demise years is expected to reveal the dominant mechanisms behind the variation in interannual precipitation and its spatial heterogeneity.

3. Results

3.1. Evolution of the SASM system and precipitation over the SCTP

The climatological onset/demise dates of the SASM during 1979–2015 are identified as 18 May (SASM-OD) and 17 September (SASM-DD), respectively (Figure S2), being consistent with those identified by previous studies (Wang and Linho 2002, Zhang *et al* 2017). For describing the influence of the SASM on precipitation over the SCTP, the spatial propagation of precipitation in this region is investigated. The results indicate that the SASM breaks out and lands first in the north of BOB (figure 1), and then the Himalayas block and divide it into two branches: (a) the northern branch penetrates into the inland from the southeastern corner of the SCTP, which receives a weak (2–8 mm d^{-1}) precipitation, being 1–2 d later than the SASM-OD; and (b) the western branch moves along the southern bound of the Himalayas and penetrates into the southwestern corner of the SCTP. After late June (around 28 June), precipitation starts over the whole SCTP. Likewise, the SASM withdraws reversely, accompanied by a decline in precipitation from the west (around 17 September) to the east of the SCTP (figure S4). The precipitation ends in mid-October (around 12 October) throughout the SCTP, declaring the complete retreat of the SASM in this region.

The spatial patterns of the climatological OD, DD, SL, and SP of precipitation over the SCTP during 1979–2015 are shown in figures 2(a)–(d). The OD of the precipitation delays gradually from the southeastern SCTP (around 19 May) to the western SCTP (around 28 June), while the DD of the precipitation delays in reverse from the western SCTP (around 17 September) to the southeastern SCTP (around 12 October). Correspondingly, precipitation has the longest duration (i.e. SL) and the largest amount (i.e. SP) in the southeastern TP, and the duration progressively shortens from the southeast to northwest of the SCTP, along with the decreasing SP.

The above results clearly reveal the significant spatial heterogeneity of the evolution of the SASM system and the seasonal variations in precipitation over the SCTP. Considering the precipitation propagation path that goes from the southeast and southwest corners to the inland of the SCTP (figure 1), three local regions (shown in figure 2(a)) are selected to discuss the spatial heterogeneity in precipitation characteristics in detail. They are southeastern TP (SETP), central TP (CETP), and southwestern TP (SWTP). Table 1 shows the difference in the climatological OD/DD of precipitation among the three regions. Compared with the SASM-OD (on 18 May), the climatological OD of precipitation delays by about 1, 14, and 30 d in the SETP (on 19 May), CETP (on 1 June), and SWTP (on 17 June), respectively, due to the long-distance transport of water vapor from the BOB. The climatological DD of precipitation in the SWTP (on 17 September) is the same as the SASM-DD, but that in the CETP (on 23 September) and SETP (on 30 September) is 6 and 13 d later than the SASM-DD. Precipitation has longer duration and larger amount in the SETP than that in the CETP. However, precipitation in the SWTP, with the shortest duration among the three regions, has larger (smaller) amount than that in the CETP (SETP).

For further investigating the associations between the onset and demise of the SASM and the precipitation over the SCTP, the partial correlations between the SASM-OD and SASM-DD and the four indexes (OD, DD, SL, and SP) of each grid precipitation in this region are analyzed. Figures 2(e)–(h) indicate that the SASM-OD has significant correlations

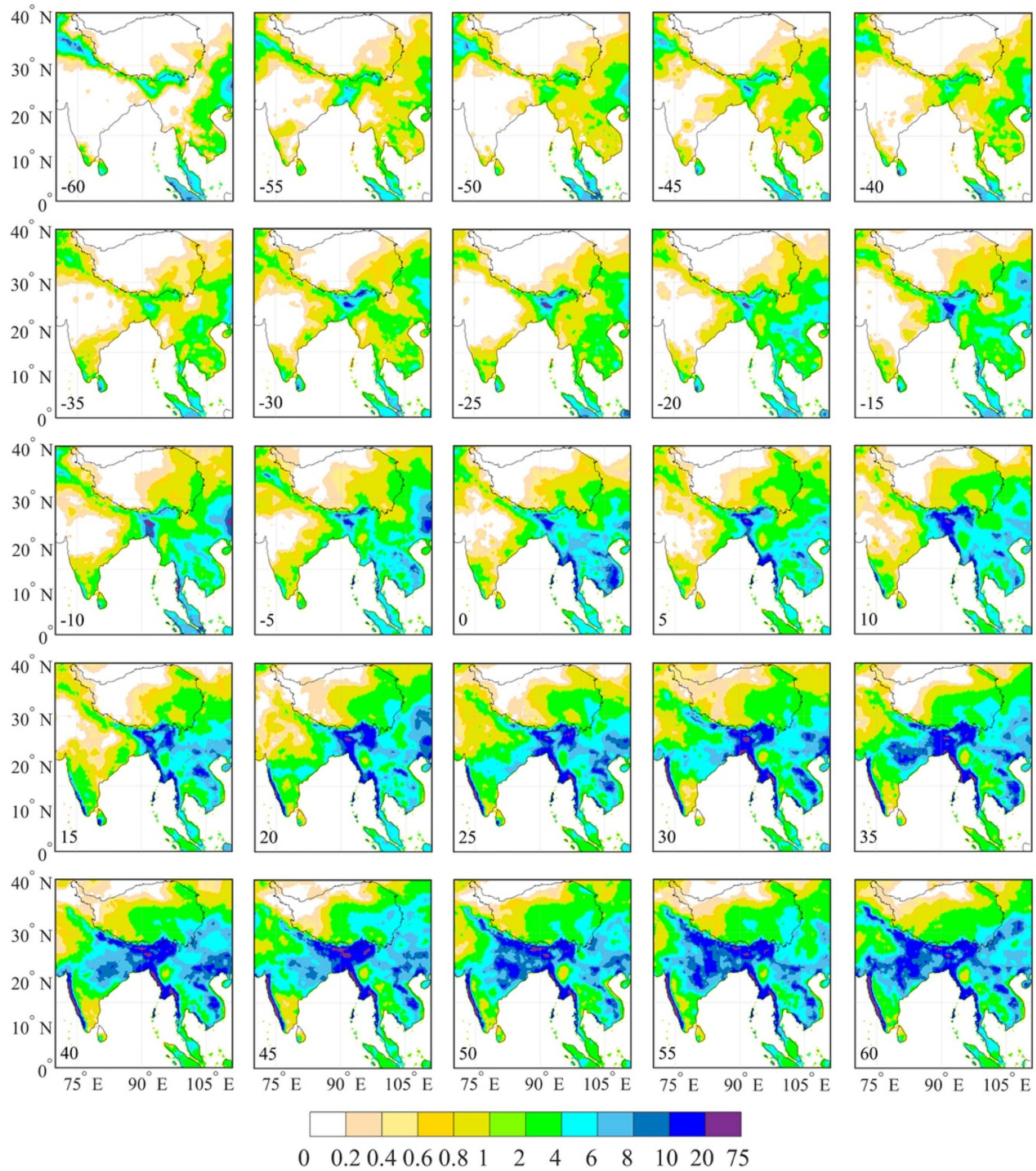

Figure 1. Evolution of climatological daily precipitation at intervals of 5 d centered on the onset date (18 May) of the South Asian summer monsoon (SASM). Units: mm d^{-1}.

with the OD, SL, and SP of precipitation over the whole SCTP, except the SWTP, reflecting the strong connections between the onset of the SASM and precipitation in this region. The SASM-DD has a positive correlation with the DD of precipitation mainly in the western and central SCTP (figures 2(j)–(l)), while there are only small areas where the SASM-DD and the SL and SP of precipitation display significant correlations (figures 2(k) and (l)), implying the weaker relationships between precipitation over the SCTP and the demise of the SASM. Besides, there are no significant correlations between the SASM-OD (SASM-DD) and the DD (OD) of precipitation over the SCTP (figures 2(f) and (i)), implying their weak connections.

The above results overall reflect the connections between the SASM and the propagation, duration, and total amount of precipitation over the SCTP, but with significant spatial heterogeneity. The results also indicate that the interannual variations (especially the duration and amount) in precipitation in the study area have stronger associations with the SASM-onset than with the SASM-demise.

3.2. Precipitation changes over the SCTP in the anomalous SASM years

In order to clarify how the anomalous onset and demise of the SASM influence the variations in interannual precipitation over the SCTP, we compare

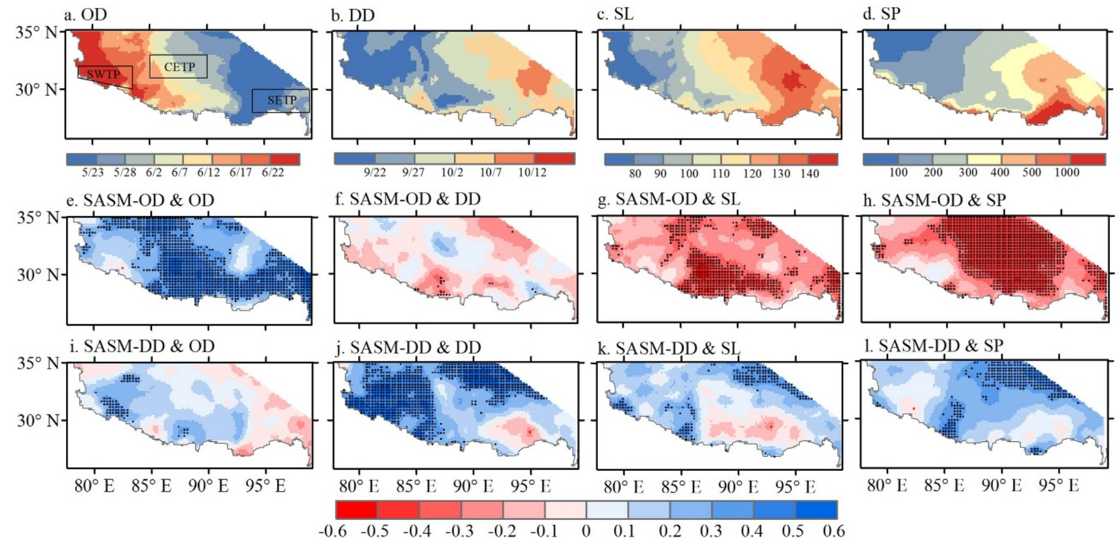

Figure 2. Climatological (a) onset date (OD), (b) demise date (DD), (c) monsoon season length (SL, in days), and (d) seasonal precipitation (SP, mm) at each grid over the South-Central Tibetan Plateau (SCTP); and the partial correlation coefficients between the onset (SASM-OD, (e)–(h)) and demise (SASM-DD, (i)–(l)) of the South Asian summer monsoon (SASM) and the above four indexes of each grid precipitation over the SCTP. The three black boxes from the west to the east (in (a)) are chosen and denoted as the southwestern Tibetan Plateau (SWTP) (30°–32°N, 78.5°–83.5°E), central Tibetan Plateau (CETP) (31°–33°N, 85°–90°E), and the southeastern Tibetan Plateau (SETP) (28°–30°N, 94°–99°E), respectively. The black dots indicate the significant correlations at the 95% confidence level.

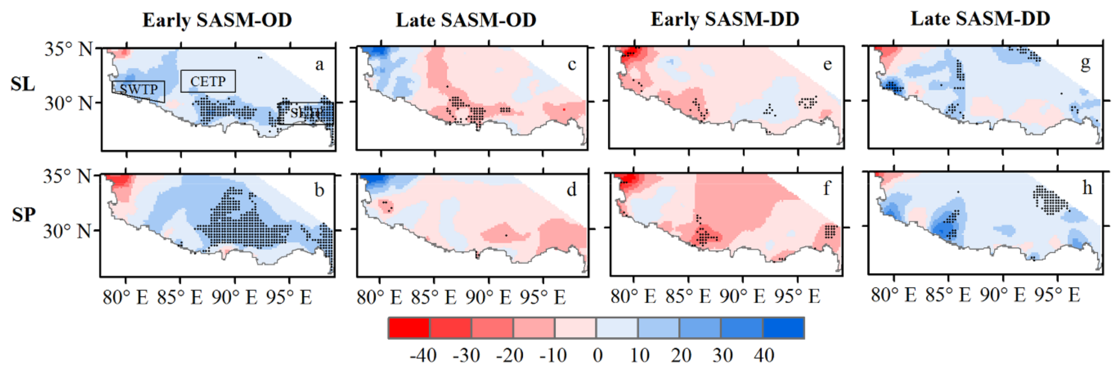

Figure 3. Composite difference in the monsoon season length (SL) and seasonal precipitation (SP) at each grid over the South-Central Tibetan Plateau (SCTP) between the early (late) and climatological SASM-onset (SASM-OD) and SASM-demise (SASM-DD) years, unit: (%). The black dots indicate the significant changes at the 95% confidence level by the *t* test. The three local regions are the same as those in figure 2

the relative changes in precipitation (both duration and total amount) in the early (late) SASM-onset (-demise) years with their climatology (see figure 3).

Compared with the climatology, the SL in the early SASM-onset years extends over the SCTP, leading to an overall increase in the SP (figures 3(a) and (b)); however, in the late SASM-onset years, the SL becomes shorter and the SP decreases (figures 3(c) and (d)). Specifically, in the SETP, there are symmetric anomalies in the SL (7.96% versus 7.36%) and SP (11.19% versus 12.22%) between the early SASM-onset years and the late SASM-onset years (table 1). In the CETP, the changes in the SL (4.69% versus 2.32%) and SP (14.62% versus 1.29%) in the early SASM-onset years are larger than those in the late SASM-onset years (table 1). In the SWTP, there are also larger changes in the SL (10.26% versus 5.63%) and SP (4.76% versus 2.80%) in the early SASM-onset years than those in the late SASM-onset years (table 1).

In the early (late) SASM-demise years, the SL shortens (extends) and the SP decreases (increases) over the SCTP when compared with the climatology (figures 3(e)–(h)). In the SETP, the changes in the SL (1.29% versus 6.89%) generate a 5.81% (7.24%) decrease (increase) in the SP in the early (late) SASM-demise years (table 1). In the CETP, the SL becomes shorter (longer) by 1.44% (7.34%), causing 14.10% (7.40%) changes in the SP in the early (late) SASM-demise years. In the SWTP, the anomaly of the SL (11.30% versus 24.40%) and SP (9.53% versus 20.33%) in the early SASM-demise years are

Table 1. Climatological onset date (OD), demise date (DD), monsoon season length (SL), and seasonal precipitation (SP), and their anomalies in the early and late SASM-onset (SASM-OD) and SASM-demise (SASM-DD) years in the southeastern Tibetan Plateau (SETP), central Tibetan Plateau (CETP), and southwestern Tibetan Plateau (SWTP).

		OD		DD		SL		SP	
Region	Phase	Date (Julian Day)	Absolute Change (Days)	Date (Julian Day)	Absolute Change (Days)	Days	Relative Change (%)	Amount (mm)	Relative Change (%)
SETP	Climatology	140 (19 May)		274 (30 September)		135		667.19	
	Early SASM-OD	130	−10	275	1	145	7.96	741.83	11.19
	Late SASM-OD	150	10	275	1	125	−7.36	585.63	−12.22
	Early SASM-DD	141	1	273	−1	133	−1.29	628.41	−5.81
	Late SASM-DD	138	−2	282	8	144	6.89	715.49	7.24
CETP	Climatology	153 (1 June)		267 (23 September)		114		226.22	
	Early SASM-OD	143	−9	262	−4	119	4.69	259.29	14.62
	Late SASM-OD	155	3	267	0	111	−2.32	223.30	−1.29
	Early SASM-DD	152	−1	264	−3	112	−1.44	194.32	−14.10
	Late SASM-DD	153	0	275	8	122	7.34	242.96	7.40
SWTP	Climatology	169 (17 June)		261 (17 September)		91		287.43	
	Early SASM-OD	159	−11	258	−1	100	10.26	301.13	4.76
	Late SASM-OD	165	−4	261	1	96	5.63	295.48	2.80
	Early SASM-DD	155	−14	236	−24	80	−11.30	260.04	−9.53
	Late SASM-DD	166	−3	279	19	113	24.40	345.87	20.33

smaller than those in the late SASM-demise years (table 1).

By comparing the early and late SASM-onset years, there is a difference of 15.32%, 7.01%, and 4.63% in the SL, and a difference of 23.41%, 15.91%, and 1.96% in the SP in the SETP, CETP, and SWTP, respectively. Between the early and late SASM-demise years, there is a difference of 8.17%, 8.79%, and 35.70% in the SL, and a difference of 13.05%, 21.50%, and 29.86% in the SP in the SETP, CETP, and SWTP, respectively.

The above results clearly indicate the asymmetric effects of the anomalous SASM and their spatial heterogeneity. To be specific, (a) the anomalous onset of the SASM leads to larger (smaller) precipitation anomalies over the SETP (CETP and SWTP) when compared with its anomalous demise; (b) there is a westward strengthening effect of the SASM-onset anomaly, but an eastward weakening effect of the SASM-demise anomaly over the SCTP; (c) the early onset of the SASM causes larger precipitation anomalies over the CETP and SWTP than its late onset, while there is an asymmetry between the early and late onset of the SASM over the SETP, causing similar precipitation anomalies over this region; and (d) the early demise of the SASM causes larger precipitation anomalies over the CETP than its late demise, while the opposite occurs over the SETP and SWTP.

3.3. Mechanisms governing the interannual precipitation variation over the SCTP

By comparing the time series of daily precipitation in the climatological and anomalous SASM years (figures S5 and S6), it can be seen that the precipitation amount has strong differences during the onset (May and June) and demise (September and October) phases of the SASM, versus only weak difference during the SASM-prevailing period (July and August). This implies that the anomalies in the duration and amount of precipitation mainly occur during the onset and demise phases of the SASM. This phenomenon is also confirmed by the similarity between the precipitation changes during the onset or demise phases (table S2) and the total precipitation changes (in table 1). Thus, to explore the physical mechanisms governing the precipitation anomaly over the SCTP, we analyze the water vapor transport and the moisture budget changes during the onset and demise phases of the SASM.

Figure 4 (and figure S7) shows the water vapor transport at 500hPa (left column) and 850hPa (right column) levels in the climatological and anomalous onset/demise phases of the SASM. In climatological status, the southwesterly monsoon flow brings warm and moist air from the Indian Ocean through the BOB and into the SCTP, acting as the main source of precipitation in this region. The upward water vapor transport is intensive along the southern boundaries of the SCTP forced by the rough topography (i.e. the Himalayas), contributing to the formation of precipitation over this region. Precipitation in the SETP and SWTP is under the combined influence of water vapor transport in both horizontal and vertical directions. The water vapor from the southern channel enters the SETP through the Yarlung Tsangpo Grand Canyon from southwest to northeast and goes upward when hindered by the high topography, while the water vapor in the SWTP comes from the western channel of water vapor transport and is lifted due to the barrier of the Himalayas (figures 4(a), (d) and S7(a), (d)). Owing to the high altitude of the TP, the flow facilitates the water vapor northward into the CETP mainly above the 500hPa level, but the upward motion of the water vapor transport is not active in this region (figures 4(a), (d) and S7(a), (d)).

The results from the moisture budget analysis during the onset and demise phases of the SASM are shown in figures 5 and S8. The results confirm that the horizontal moisture convergence (figures 5(b) and S8(b)) plays a dominant role in precipitation formation over the wide plateau on the north of the Himalayas, while the vertical moisture convergence (figures 5(c) and S8(c)) is also an important contributor to the precipitation in the southern Himalayas due to the topographic effect, as already documented previously (Dong et al, 2016). However, the surface evaporation contributes little to the precipitation over the whole SCTP (figures 5(d) and S8(d)).

Given the characteristics of the water vapor transport and the moisture budget, we further examine their changes during the anomalous SASM-onset (and -demise) phases to understand the precipitation anomaly over the SCTP. The results show that the SASM-prevailing area is characterized by the cyclonic (anticyclonic) water vapor transport generated by anomalous SASM activity during the early (late) SASM-onset phases, leading to the moisture convergence (divergence) with intensive upward (downward) motion in this region (figures 4(b), (c), (e), (f) and S7(b), (c), (e), (f)). Additionally, the topographic effect also accounts for the anomaly in water vapor transport in the vertical direction and contributes to the moisture convergence (divergence) over the SETP and SWTP when compared with that over the CETP (figures 4(b), (c), (e), (f) and S7(b), (c), (e), (f)). Similar patterns of water vapor transport and moisture budget changes can also be found during the anomalous SASM-demise phases, but the magnitude of the changes is weaker than that during the anomalous SASM-onset phases (figures S7 and S8).

Overall, the anomalies in the total moisture convergence (figures 5(e), (k) and S8(e), (k)) spatially match well with the precipitation anomaly

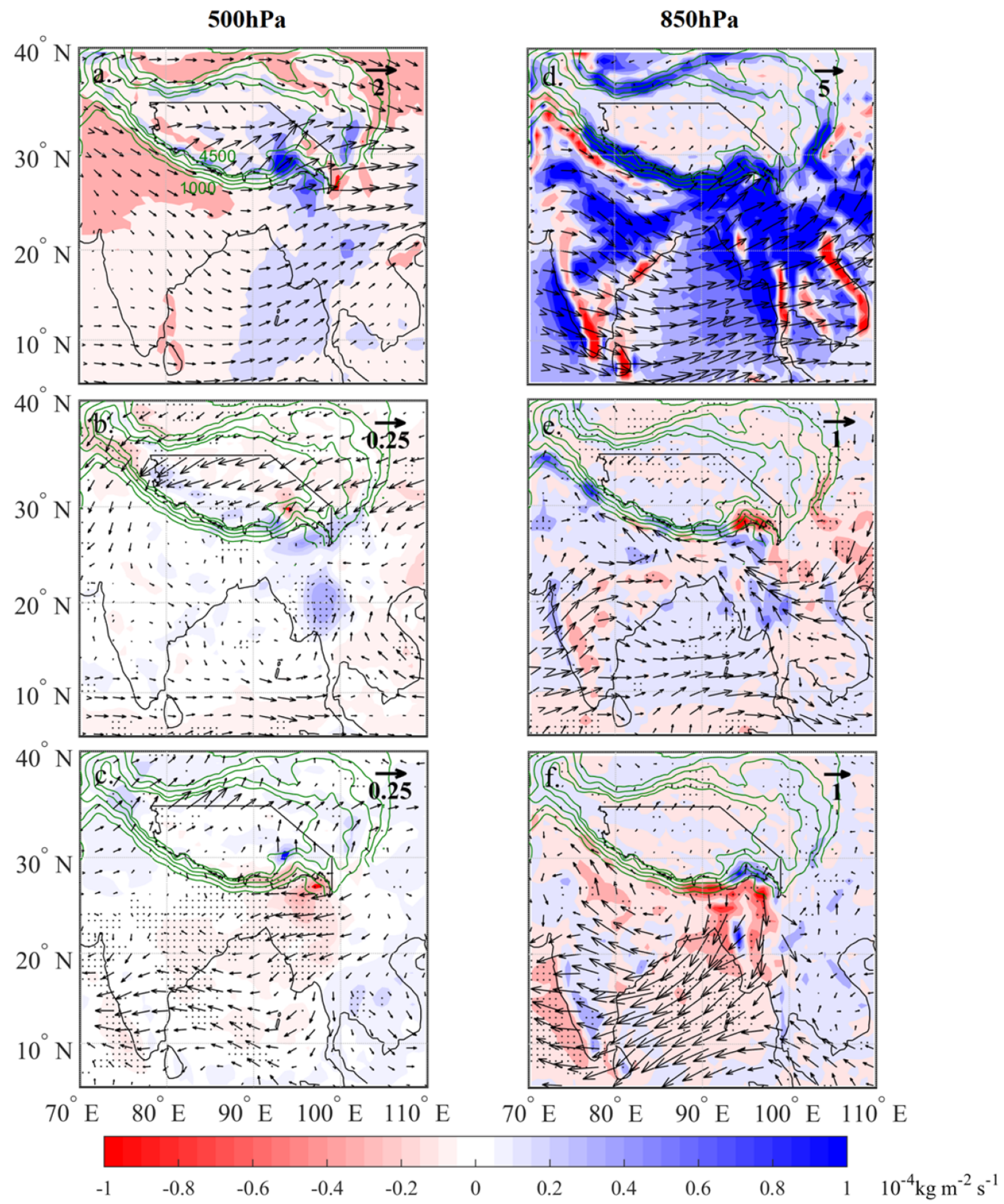

Figure 4. The horizontal (vectors, unit: 10^{-3}kg m^{-1} hpa^{-1} s^{-1}) and vertical (shaded, unit: 10^{-4}kg m^{-2} s^{-1}) water vapor transport during the climatological (a), (d) onset phases of the South Asian summer monsoon (SASM) at 500hPa (left column) and 850hPa (right column), respectively. The composite difference in the horizontal and vertical water vapor transport between early and climatological (b), (e), and between late and climatological (c), (f) onset phases of the SASM at 500hPa (left column) and 850hPa (right column), respectively. The black dots indicate the significant changes at the 95% confidence level by the *t* test. The green lines show the contours of the Tibetan Plateau with 1000 m interval.

(figures 3(b), (d), (f), (h)), suggesting the dominant physical contribution of the moisture convergence anomaly, including both moisture and wind flow changes. However, the weak surface evaporation anomalies contribute little to the precipitation anomaly (figures 5(j), (p) and S8(j), (p)). Thus, the contributions of the anomalies in the horizontal thermodynamic component (i.e. the horizontal moisture), horizontal dynamic component (i.e. the horizontal wind flow), vertical thermodynamic component (i.e. the vertical moisture), and vertical dynamic component (i.e. the vertical wind flow) are quantified as major factors governing precipitation anomaly and its spatial heterogeneity over the SCTP (figures 5(f)–(i), (l)–(o), and figures S8(f)–(i), (l)–(o)).

We take the three regions as examples again to explain the precipitation anomaly. The results are shown in figure 6 (and table S2). Over the SETP, the significant changes in both the horizontal and vertical

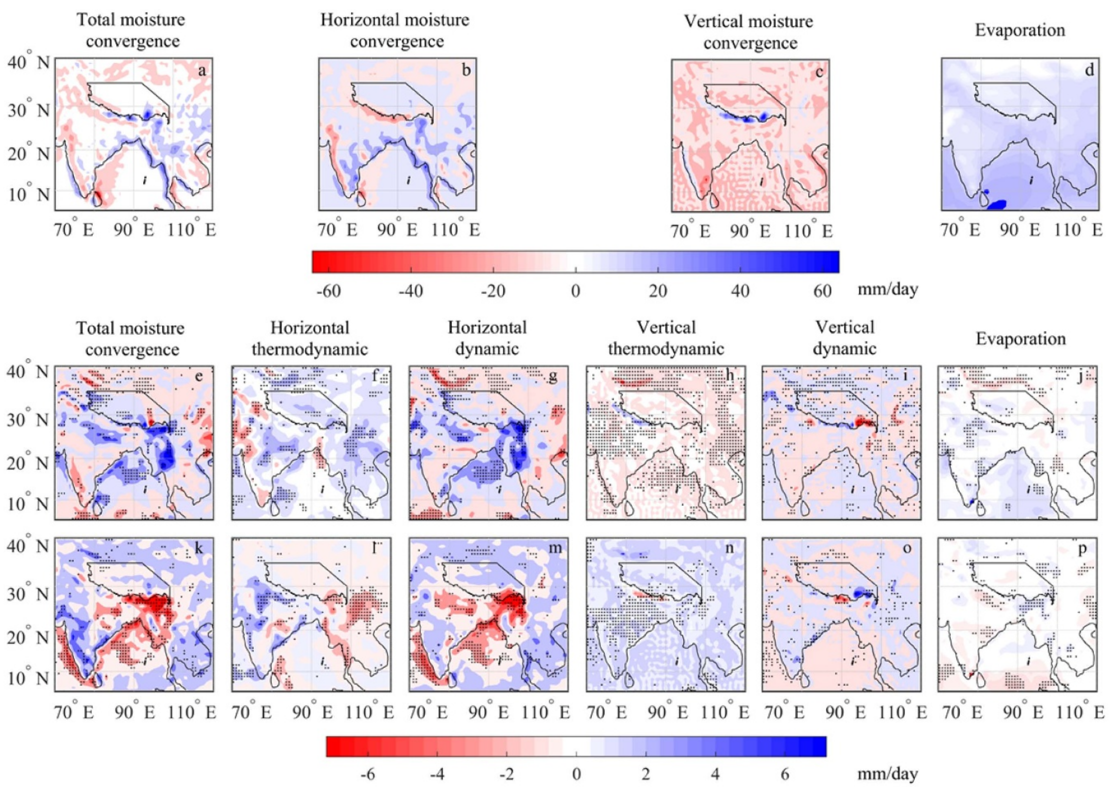

Figure 5. Climatology of (a) the total moisture convergence, (b) the horizontal moisture convergence, (c) the vertical moisture convergence, and (d) the surface evaporation during the onset phase (May and June) of the SASM. The composite difference in the total moisture convergence, horizontal thermodynamic component, horizontal dynamic component, vertical thermodynamic component, vertical dynamic component, and surface evaporation between early and climatological (e)–(j), and between late and climatological (k)–(p) onset phases of the SASM. The black dots indicate the significant changes at the 95% confidence level by the *t* test.

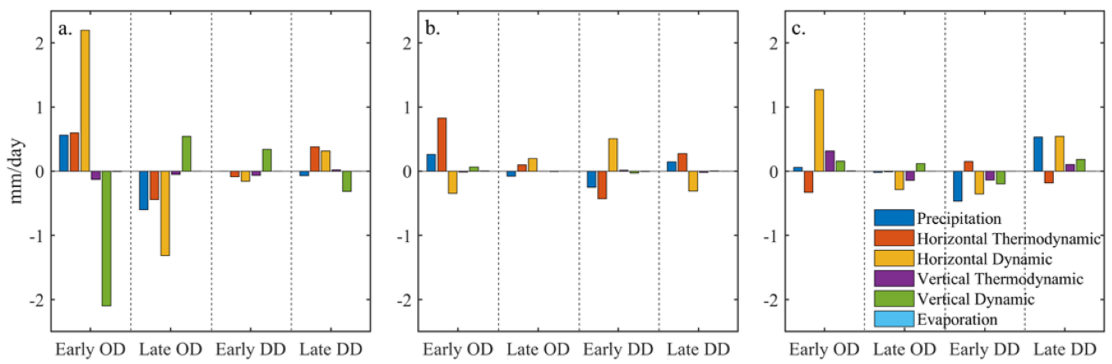

Figure 6. Composite difference in precipitation and moisture budget components between early and climatological, and late and climatological SASM-onset (-demise) years in (a) the southwestern Tibetan Plateau (SWTP), (b) the central Tibetan Plateau (CETP), and (c) the southeastern Tibetan Plateau (SETP).

dynamic components, together with a smaller change in the horizontal thermodynamic component, lead to the precipitation anomaly in the anomalous SASM years, but the vertical thermodynamic component contributes only little. Over the CETP, the precipitation anomaly is mainly caused by the large changes in the horizontal thermodynamic component, and also the smaller changes in the horizontal dynamic component in the anomalous SASM years, whereas the vertical thermodynamic and dynamic components contribute very little due to their small changes. The precipitation anomaly over the SWTP is attributed to the notable changes in all the four components in the anomalous SASM years.

By further comparing the changes in the four components in the early and late SASM-onset (-demise) years, the physical mechanisms involved in the asymmetric effects of the anomalous SASM are explained. Over the SETP, we find that smaller changes (0.09–0.34 mm d^{-1}) in the horizontal thermodynamic and dynamic components, as well as the negative effects of the vertical dynamic component, cause smaller precipitation anomalies in the early SASM-demise years compared with those (0.31–0.38 mm d^{-1}) in the late SASM-demise years. Over the CETP, the changes (0.34–0.83 mm d^{-1}) in the horizontal thermodynamic and dynamic components in the early SASM-onset years are rather larger than those (0.10–0.19 mm d^{-1}) in the late SASM-onset years, generating a larger precipitation anomaly in the former. Further, larger changes (0.43–0.51 mm d^{-1}) in the early SASM-demise years than those of the late SASM-demise years (0.28–0.31 mm d^{-1}) also mirror the precipitation anomalies in this region. Over the SWTP, larger changes in the horizontal dynamic component, combined with smaller changes in the other three components (0.16–1.27 mm d^{-1}), lead to a larger precipitation anomaly in the early SASM-onset years compared with those (0.01–0.28 mm d^{-1}) in the late SASM-onset years. Further, smaller changes (0.14–0.36 mm d^{-1}) in the four components in the early SASM-demise years also lead to smaller precipitation anomalies compared with those (0.10–0.54 mm d^{-1}) in the late SASM-demise years over the SWTP.

Moreover, there is an average difference of 2.40 mm d^{-1}, 0.63 mm d^{-1}, and 0.59 mm d^{-1} in the moisture budget components between the early and late SASM-onset years in the SETP, CETP, and SWTP, respectively. There is also an average difference of 0.53 mm d^{-1}, 0.76 mm d^{-1}, and 0.86 mm d^{-1} between the early and late SASM-demise years in the SETP, CETP, and SWTP, respectively. Besides, large (small) changes in the moisture budget components reasonably explain the larger (smaller) precipitation anomalies in the anomalous SASM-onset years versus those in the SASM-demise years in the SETP (CETP and SWTP).

Overall, the above results indicate that the precipitation anomaly over the SCTP is linked with the cyclonic and anticyclonic water vapor transport generated by the anomalous SASM activity during its onset and demise phases. Furthermore, the amplitude difference in the moisture budget generated by the horizontal and vertical thermodynamic and dynamic processes explains the asymmetric effects of the SASM between its onset and demise, and between its early and late onset (demise), which further determine the precipitation anomaly and its spatial heterogeneity over the SCTP.

4. Conclusions

In this study, the influences of the anomalous onset and demise of the SASM system on the interannual variations in precipitation over the SCTP have been examined, and the changes in water vapor transport and moisture budgets have been analyzed to explain the physical causes. The results show the dominant role of the SASM on the propagation, duration, and total amount of precipitation over the SCTP. The results also indicate that the duration and total amount of precipitation over the SCTP have more significant correlations with the onset of the SASM rather than with its demise, implying stronger connections with the onset of the SASM, but with significant spatial heterogeneity.

Furthermore, it has been found that the precipitation anomaly over the SCTP is dominated by the cyclonic and anticyclonic water vapor transport associated with the anomalous SASM activities, leading to the moisture convergence and divergence with intensive upward and downward motion. The topographic effect further strengthens the anomaly in water vapor transport in the vertical direction and contributes to the moisture convergence and divergence in the SETP and SWTP, rather than in the CETP. There are asymmetric effects of the SASM with topography between onset and demise, and between early and late onset (demise) of the SASM, which generates the asymmetric precipitation anomaly over the SCTP by regulating the horizontal and vertical thermodynamic and dynamic processes, along with evident spatial heterogeneity.

In summary, the water vapor transport and its changes generated by the SASM, combined with the topographic effect, control the precipitation propagation and its anomaly across the SCTP. The results presented here would be helpful to improve our understanding of the SASM-precipitation relationship over the SCTP and can also guide planning and management of the freshwater resources in the SCTP and its surrounding areas. Further advances in research in this region can involve study of the precipitation extremes in anomalous SASM years, as well as their potential influences on the mountain floods, landslides, mudslides, and other relevant natural disasters over the SCTP.

Data availability statement

All data that support the findings of this study are included within the article (and any supplementary information files).

Acknowledgments

This project was financially supported by the Second Tibetan Plateau Scientific Expedition and Research Program (STEP) (No. 2019QZKK0903), the Strategic Priority Research Program of Chinese Academy of Sciences (No. XDA20060402), the National Natural Science Foundation of China (Nos. 91647110, 41971040), and the Youth Innovation Promotion Association CAS (No. 2017074), as well as the Swedish National Space Agency (SNSA: 188/18), the Swedish Research Council (VR: 2019-03954), and the CAS Interdisciplinary Innovation Team

(No. JCTD-2019-04). The data were obtained from APHRODITE's Water Resources (https://www.chikyu.ac.jp/precip/products.html) and the European Centre for Medium-Range Weather Forecasts (https://www.ecmwf.int/). The authors gratefully acknowledge the valuable comments and suggestions given by the Editor and the anonymous reviewers on earlier versions, which led to significant improvements to the presentation of the work performed.

ORCID iDs

Yanxin Zhu https://orcid.org/0000-0002-8192-4285
Yan-Fang Sang https://orcid.org/0000-0001-6770-9311
Deliang Chen https://orcid.org/0000-0003-0288-5618
Bellie Sivakumar https://orcid.org/0000-0003-0523-890X
Donghuan Li https://orcid.org/0000-0001-5960-3816

References

Chen B, Xu X-D, Yang S and Zhang W 2012 On the origin and destination of atmospheric moisture and air mass over the Tibetan Plateau *Theor. Appl. Climatol.* **110** 423–35
Chen X and You Q 2017 Effect of Indian Ocean SST on Tibetan Plateau precipitation in the early rainy season *J. Clim.* **30** 8973–85
Cherchi A, Alessandri A, Masina S and Navarra A 2011 Effects of increased CO_2 levels on monsoon *Clim. Dyn.* **37** 83–101
Curio J and Scherer D 2016 Seasonality and spatial variability of dynamic precipitation controls on the Tibetan Plateau *Earth Syst. Dyn.* **7** 767–82
Dong W *et al* 2016 Summer rainfall over the southwestern Tibetan Plateau controlled by deep convection over the Indian subcontinent *Nat. Commun.* **7** 10925–10925
Fasullo J T and Webster P J 2003 A hydrological definition of indian monsoon onset and withdrawal *J. Clim.* **16** 3200–11
Feng L and Zhou T 2012 Water vapor transport for summer precipitation over the Tibetan Plateau: multidata set analysis *J. Geophys. Res.* **117** D20114
Goswami B N and Xavier P K 2005 ENSO control on the south Asian monsoon through the length of the rainy season *Geophys. Res. Lett.* **32** L18717
Immerzeel W, van Beek L P H and Bierkens M F P 2010 Climate change will affect the Asian water towers *Science* **328** 1382–5
Li C F and Yanai M 1996 The onset and interannual variability of the Asian summer monsoon in relation to land–sea thermal contrast *J. Clim.* **9** 358–75
Liu Y, Chen H, Zhang G, Sun J and Wang H 2019 The advanced South Asian monsoon onset accelerates lake expansion over the Tibetan Plateau *Sci. Bull.* **64** 1486–9
Ma Y Z, Lu M Q, Chen H N, Pan M X and Hong Y 2018 Atmospheric moisture transport versus precipitation across the Tibetan Plateau: a mini-review and current challenges *Atmos. Res.* **209** 50–58
Misra V, Bhardwaj A and Mishra A 2018 Local onset and demise of the Indian summer monsoon *Clim. Dyn.* **51** 1609–22
Noska R and Misra V 2016 Characterizing the onset and demise of the Indian summer monsoon *Geophys. Res. Lett.* **43** 4547–54
Pai D S and Bhan S C 2014 Monsoon 2013: a report (IMD Met. Monograph No: ESSO/IMD/SYNOPTICMET/01-2014/15). Pune, India: India Meteorological Department, National Climate Center
Pai D S and Bhan S C 2015 Monsoon 2014: a report (IMD Met. Monograph No: ESSO/IMD/SYNOPTIC MET/01(2015)/17). Pune, India: India Meteorological Department, National Climate Center
Roxy M K, Ritika K, Terray P, Murtugudde R, Ashok K and Goswami B N 2015 Drying of Indian subcontinent by rapid Indian Ocean warming and a weakening land-sea thermal gradient *Nat. Commun.* **6** 7423
Sabeerali C T and Ajayamohan R S 2018 On the shortening of Indian summer monsoon season in a warming scenario *Clim. Dyn.* **50** 1609–24
Sabeerali C T, Rao S A, Ajayamohan R S and Murtugudde R 2012 On the relationship between Indian summer monsoon withdrawal and Indo-Pacific SST anomalies before and after 1976/1977 climate shift *Clim. Dyn.* **39** 841–59
Sang Y F, Singh V P, Gong T, Xu K, Sun F, Liu C, Liu W and Chen R 2016 Precipitation variability and response to changing climatic condition in the Yarlung Tsangpo River basin, China *J. Geophys. Res.* **121** 8820–31
Schiemann R, Lüthi D and Schär C 2009 Seasonality and interannual variability of the westerly jet in the Tibetan Plateau region *J. Clim.* **22** 2940–57
Seager R and Henderson N 2013 Diagnostic computation of moisture budgets in the ERA-interim reanalysis with reference to analysis of CMIP-archived atmospheric model data *J. Clim.* **26** 7876–901
Seager R, Naik N and Vecchi G A 2010 Thermodynamic and dynamic mechanisms for large-scale changes in the hydrological cycle in response to global warming *J. Clim.* **23** 4651–68
Tong K, Su F, Yang D, Zhang L and Hao Z 2014 Tibetan Plateau precipitation as depicted by gauge observations, reanalysis and satellite retrievals *Int. J. Climatol.* **34** 265–85
Trenberth K E and Guillemot C J 1995 Evaluation of the global atmospheric moisture budget as seen from analyses *J. Clim.* **8** 2255–72
Walker J M and Bordoni S 2016 Onset and withdrawal of the large-scale South Asian monsoon: a dynamical definition using change point detection *Geophys. Res. Lett.* **43** 11–815
Wang A and Zeng X 2012 Evaluation of multireanalysis products with in situ observations over the Tibetan Plateau *J. Geophys. Res.* **117** D5
Wang B and Linho 2002 Rainy seasons of the Asian-Pacific summer monsoon *J. Clim.* **15** 386–98
Wang B, Wu R and Lau K-M 2001 Interannual variability of the Asian summer monsoon: contrasts between the Indian and the western North Pacific–East Asian monsoons *J. Clim.* **14** 4073–90
Webster P J, Magana V O, Palmer T N, Shukla J, Tomas R A, Yanai M U and Yasunari T 1998 Monsoons: processes, predictability, and the prospects for prediction *Clim. Dyn.* **103** 14451–510
Xavier P K, Marzin C and Goswami B N 2007 An objective definition of the Indian summer monsoon season and a new perspective on the ENSO–monsoon relationship *Q. J. R. Meteorol. Soc.* A **133** 749–64
Xiang B and Wang B 2013 Mechanisms for the advanced Asian summer monsoon onset since the mid-to-late 1990s *J. Clim.* **26** 1993–2009
Xing N, Li J, Jiang X and Wang L 2016a Local oceanic precursors for the summer monsoon onset over the Bay of Bengal and the underlying processes *J. Clim.* **29** 8455–70
Xing N, Li J and Wang L 2016b Effect of the early and late onset of summer monsoon over the Bay of Bengal on Asian precipitation in May *Clim. Dyn.* **47** 1961
Yang K, Wu H, Qin J, Lin C, Tang W and Chen Y 2014 Recent climate changes over the Tibetan Plateau and their impacts on energy and water cycle: a review *Glob. Planet. Change* **112** 79–91

Yang K, Ye B, Zhou D, Wu B, Foken T, Qin J and Zhou Z 2011 Response of hydrological cycle to recent climate changes in the Tibetan Plateau *Clim. Change* **109** 517–34

Yao T *et al* 2013 A review of climatic controls on δ^{18}O in precipitation over the Tibetan Plateau: observations and simulations *Rev. Geophys.* **51** 525–48

Yatagai A, Kamiguchi K, Arakawa O, Hamada A, Yasutomi N and Kitoh A 2012 APHRODITE: constructing a long-term daily gridded precipitation dataset for Asia based on a dense network of rain gauges *Bull. Am. Meteorol. Soc.* **93** 1401–15

Zhang W, Zhou T and Zhang L 2017 Wetting and greening Tibetan Plateau in early summer in recent decades *J. Geophys. Res.* **122** 5808–22

Zhu Y X and Sang Y F 2018 Spatial variability in the seasonal distribution of precipitation on the Tibetan Plateau (in Chinese) *Prog. Geogr.* **37** 1533–44